

Rhodium and Rhodium-Alloy Films and Nanoparticles: Part I

A review of synthesis methods

Yicheng Zhou, Wangping Wu*

Electrochemistry and Corrosion Laboratory,
School of Mechanical Engineering and Rail
Transit, Changzhou University, Changzhou
213164, China

Qinqin Wang

School of Mechanical Engineering, Yangzhou
University, Yangzhou 225127, China

Liangbing Wang

Avic Tianjin Aviation Electro-mechanical Co Ltd,
Tianjin 300308, China

*Email: wwp3.14@163.com;
wuwping@cczu.edu.cn

PEER REVIEWED

Received 24th October 2022; Revised 28th
February 2023; Accepted 20th March 2023;
Online 22nd March 2023

Noble metals are key to various research fields and noble metal nanomaterials are directly relevant to optics, catalysis, medicine, sensing and many other applications. Rhodium-based nanomaterials have been less studied than metals such as gold, silver or platinum. There have been many improvements in characterisation tools over the years and knowledge about rhodium chemistry and nanomaterials is growing rapidly. Rhodium nanoparticles are widely used as catalysts for automotive emissions control and for hydrogen and oxygen precipitation reactions in electrolytic cells. Novel applications in electronics, anticancer drugs and aerospace are being revisited. In Part I of this

two-part review, we cover different strategies for the synthesis of rhodium films and nanoparticles.

1. Introduction

Nanomaterials have attracted increasing interest over the years (1). At a scale between molecules and bulk materials, nanostructures present a range of unique properties which can be finely controlled for specific purposes (2). Nanomaterials made of gold, silver, platinum, palladium, ruthenium, rhodium, iridium or osmium have proved an efficient way to make the most of these metals with optimisation down to the atomic scale (3). This is a much-needed strategy since noble metals are critical raw materials for multiple applications. Nanomaterials with high surface-to-volume ratio also allow efficient use of atoms. This is particularly relevant for catalytic reactions where only surface atoms are directly involved in catalytic processes (4).

Noble metal nanoparticles (NMNPs) with controlled sizes and shapes have drawn increased scientific interest and technological significance owing to their unique physical and chemical properties and wide applications in catalysis, photonics, sensing, energy conversion/storage and biomedicine (5). NMNPs can modify their catalytic behaviour in terms of activity, selectivity and persistence by modulating the number and geometry of the active sites and even their size and shape (6, 7).

Rhodium has a cool-gray colour and is extremely hard and corrosion resistant. Like its sister metals platinum and palladium, rhodium has excellent catalytic activity. Rhodium-based catalysts are highly resistant to acids, bases and heat and are particularly stable under harsh reaction conditions. Rhodium is particularly known for its

Table I Properties of Rhodium

Rhodium	Parameter
Resistivity, ρ , Ω m at 20°C	$4.49 \times 10^{-8} \Omega$ m
Conductivity, σ , S m ⁻¹ at 20°C	$2.23 \times 10^7 S$ m ⁻¹
Density	12.41 g cm ⁻³
Hardness (Brinell value)	1100 MN m ⁻²
Melting point	1960°C
Chemical element of Group	VIII (Mendeleev)
Atomic number	45
Atomic weight	106.42
Thermal conductivity	150 W m ⁻¹ °C ⁻¹
Tensile strength (annealed condition)	71 kg mm ⁻²

key role in a variety of catalytic reactions such as CO oxidation, NO reduction, hydrogenation, hydroformylation and electrolysis of water. Today's three-way catalyst for gasoline engines commonly uses rhodium to catalyse the reduction of nitrogen oxides to nitrogen. Rhodium has high melting point, high temperature stability and corrosion resistance (Table I), which makes it a key to many industrial processes such as glass, glass fibre production, optical mirrors and sensors. Therefore, in this work, the preparation and potential applications of rhodium and rhodium-alloy thin films and nanoparticles will be reviewed.

2. Synthesis of Thin Films and Nanoparticles of Rhodium and Rhodium Alloy

Several syntheses have been reported to produce rhodium and rhodium-alloy thin films and nanomaterials. There are dry and wet synthesis methods. Compared to wet chemical synthesis, dry synthesis often requires high temperature or vacuum

processing such as magnetron sputtering (8–14) or laserpulsing (15–26) and therefore requires relatively specialist equipment. Wet chemical synthesis (for example, electrochemical synthesis (27–40)) is carried out in the liquid phase, usually by reduction of rhodium precursors. Especially in catalysis, some variables, such as size and loading, may require attention. A support is often required to stabilise the NPs and support effects cannot be ruled out when assessing catalyst performance.

2.1 Magnetron Sputtering

Magnetron sputtering is a physical vapour deposition technology (8). Due to its low temperature, high efficiency, high film forming efficiency and good film quality, it is widely used in industrial films and coatings (9, 10). During magnetron sputtering, a magnetic field between two poles is applied. Electrons are accelerated within a magnetic field. Electrons move in a cycloidal motion, which increases collision frequency with target particles and ions in the working gas. As the degree of ionisation of the working gas increases, the working gas pressure decreases. A working gas ion is accelerated by an electric field and hits the target, releasing energy, so that the target shoots atoms or ions at the target and deposits a film on its surface (11). Adhesion of thin films is an important evaluation standard. Marot *et al.* studied the adhesion of rhodium films on metallic substrates (molybdenum, copper and stainless steel) (12). Table II shows the influence of substrate, temperature and thickness on properties of rhodium films. Adhesion was increased by increasing substrate hardness, increasing deposition temperature, using rhodium implantation treatment before film deposition or depositing an interlayer.

The substrate temperature affects the properties of as-deposited film. In Figure 1(a), the dense

Table II Temperature of Deposition, Film Thickness, Substrate Roughness, Rhodium Roughness, Substrate Hardness, Substrate Young's Modulus and Rhodium Layer Critical Load Obtained After Scratch Test (12)

Substrate	T , °C	d , μ m	$R_{a\text{ Sub}}$ nm	$R_{a\text{ Rh}}$ nm	$HV_{0.1}$	Young's modulus, GPa	L_{cr} N
Mo	30	1.7	14	18	261	359	12.9 ± 0.5
Mo	30	0.2	15	15	261	359	8.8 ± 0.8
Cu	30	0.2	12	14	122	126	1.5 ± 0.2
SS FCVA	30	0.2	5	6	273	192	8.6 ± 1.3
SS	30	0.2	9	12	273	192	6.6 ± 0.4
SS	170	0.2	11	11	273	192	8.7 ± 0.9

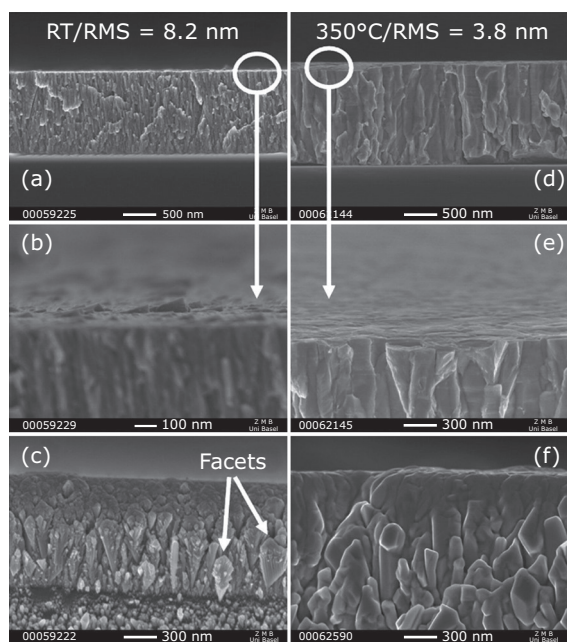


Fig. 1. Cross-sectional view of two rhodium films deposited on silicon at room temperature and 350°C: (a) room temperature sample; and (b) 350°C sample obtained after breaking the samples in the middle; (c) room temperature sample; and (d) 350°C sample recorded with a tilt of 8°; side views of naturally grown edges of the film: (e) room temperature sample; and (f) 350°C sample. Reprinted from (12) with permission from Elsevier

columnar structure of a homogeneous rhodium film with 1.2 μm thickness was deposited at room temperature. Some tips are present on the top-surface (Figure 1(b)), indicating that

the columnar structure tends to have highly faceted surface. The surface roughness (root mean square (RMS)) measured with atomic force microscope for a thick layer deposited at room temperature is around 8.2 nm. For comparison, the RMS roughness of a layer deposited at 350°C is 3.8 nm. This obvious difference in the film roughness with deposition temperature is illustrated by scanning electron microscope (SEM) images for the layer deposited at 350°C. Therefore, the dense and smooth films were obtained by magnetron sputtering.

Although rhodium nanofilms prepared by magnetron sputtering have unparalleled properties, the applications of rhodium films are ultimately limited by the high cost of rhodium. Co-deposition of rhodium-tungsten by dual magnetron sputtering was achieved by Marot *et al.* (13). X-ray photoelectron spectroscopy (XPS) or X-ray diffraction (XRD) make it possible to assess the oxidation degree of the material directly or indirectly. Illustrative examples are given in Figure 2. Figure 2(a) shows the positive shift of the core binding energy of rhodium, coupled with the shift of the rhodium *d* band, *DE_d*, away from the Fermi energy level. The negative shift of the core binding energy of tungsten is coupled with the shift of the tungsten *d* band, *DE_d*, near the Fermi energy level. Figure 2(b) shows the formation of Rh₃W phase. The reflectivity of the film decreases linearly with decreasing rhodium concentration and decreases by 13% when the tungsten concentration is 11%. Therefore, the

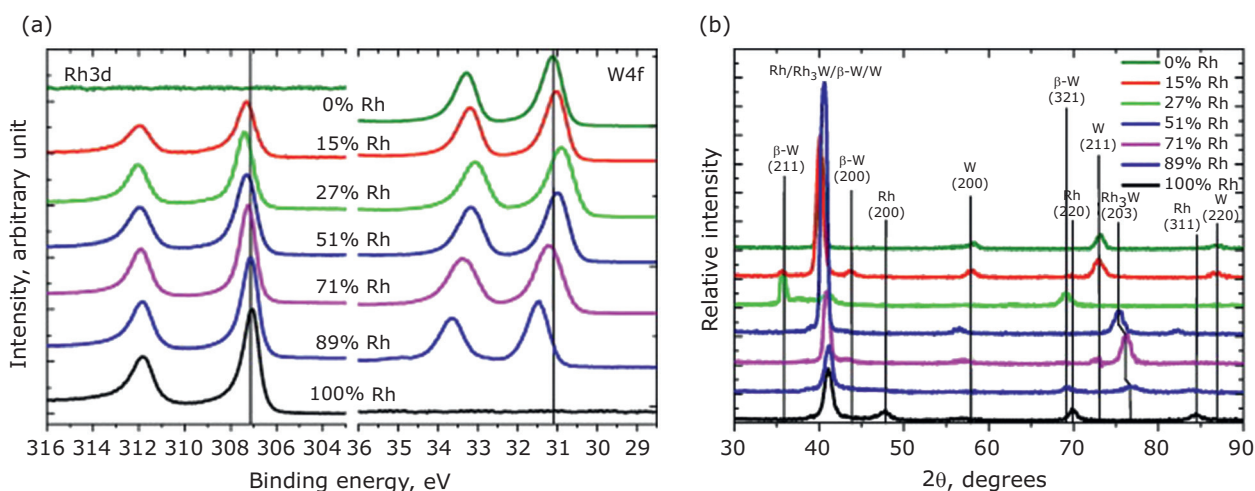


Fig. 2. (a) Rh3d and W4f core level spectra measured by *in situ* XPS on rhodium films deposited on silicon substrates with various rhodium concentrations; (b) X-ray diffraction pattern of rhodium-tungsten films deposited at room temperature on silicon with various rhodium concentrations. Reprinted from (13) with permission from Elsevier

reduction of rhodium content in the rhodium alloy has more drawbacks than benefits.

2.2 Pulsed Laser Deposition

Although rhodium can be prepared by electrochemical deposition and magnetron sputtering to obtain planar films with large and complex shape regions, there are some limitations in properly controlling the film structure and simultaneously achieving a satisfactory reflectivity behaviour at high temperature. Pulsed laser deposition (PLD) technology is a typical vapour phase deposition process for any material and can deposit a wide range of materials including metals, ceramics, ferroelectric materials, diamond-like, semiconductors, high-temperature superconducting films and even high-temperature resistant organic materials (15, 16, 19, 20). It differs from sputtering by two main features: (i) the high energy of the ejected species (ions in the keV range and neutral atoms with energies of a few eV); (ii) the high instantaneous deposition rate (a few $\text{k}\text{\AA s}^{-1}$), which favours the formation of non-equilibrium films. By varying the main process parameters, such as laser flux, background pressure and target-substrate distance, it is possible to tune the energy of the ablation species and to select the structure and morphology of the generated films, which allows the deposition of compact rhodium nanofilms with different nanostructures (18, 22). PLD allows the production of two specific structures, which have the potential to determine improved erosion properties of rhodium films: one with a highly oriented (111) polycrystalline structure and the other with an amorphous structure. The crystalline size of the highly oriented film is about 20 nm while, depending on the deposition parameters, the mean grain size of the amorphous-like film is below 10 nm (23). For comparison, a typical rhodium film deposited by magnetron sputtering has columnar morphology and randomly-oriented grains with mean dimension in the range of 10–16 nm. **Figure 3** presents a cross-sectional SEM image of rhodium film. There is a highly oriented polycrystalline columnar layer with about 200 nm thickness in the bottom third and nearly 600 nm thick amorphous film. Unlike the amorphous-like structure, the highly oriented polycrystalline structure develops compressive strains in as-deposited films which can compromise the mechanical stability of a thick film. Using multilayer films or a series of thin amorphous rhodium layers might be a reliable way to overcome this problem.

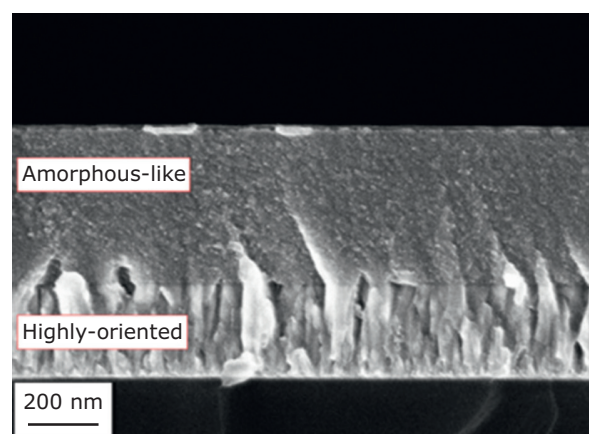


Fig. 3. SEM cross-section view of amorphous-like rhodium film with highly-oriented polycrystalline buffer. Reprinted from (23) with permission from Elsevier

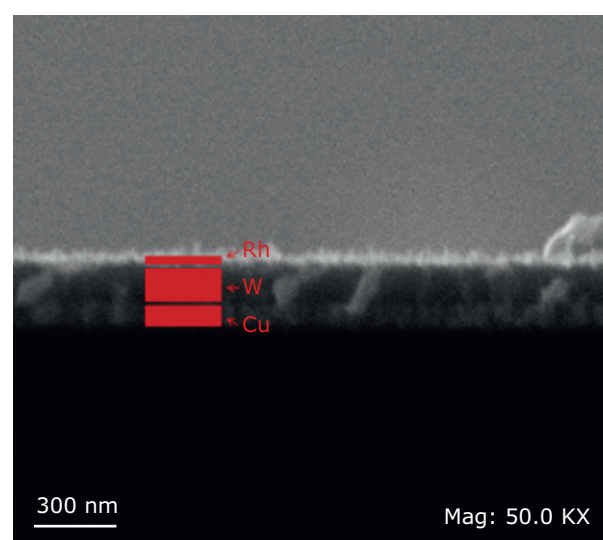


Fig. 4. Cross-sectional SEM image of multilayer thin film deposited on silicon substrate. Reprinted from (15) with permission from Elsevier

Mostako *et al.* (15) found that the quality and durability of single-layer rhodium films could be improved and the cost can be reduced by making multilayer films (**Figure 4**) by long-term exposure to fusion plasma. Passioni *et al.* (24) studied PLD rhodium film on silicon surfaces under vacuum conditions at 30 Pa. **Figure 5** shows the presence of all diffraction peaks of rhodium films deposited in vacuum. The film consists of a preferential growth in the (111) direction with a crystallite size of about 15–20 nm. With high flux, the structure of the film evolves to a crystalline shape. This confirms that the crystallinity of the film is related to the energy of the deposited species. Therefore, changing the

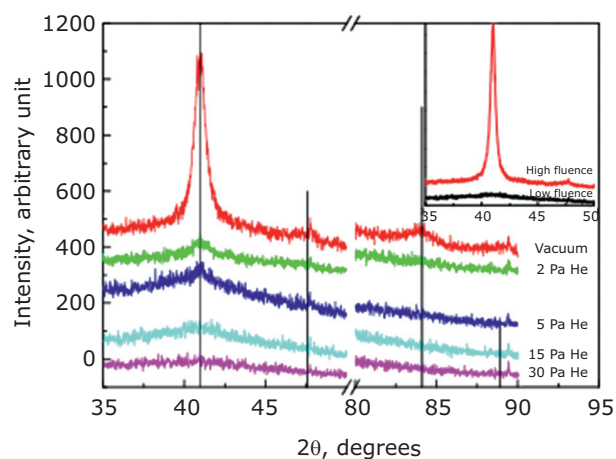


Fig. 5. XRD patterns of rhodium film obtained under varying background pressure from vacuum to 30 Pa helium. Inset: depositions made at 15 Pa at low (1.2 J cm^{-2}) and high (4.5 J cm^{-2}) flow. Reprinted from (24) with permission from Elsevier

gas pressure or laser flux has the potential to affect the nanostructure of the deposited films, which may approach the amorphous phase. In addition, PLD can influence the structure and morphology of the as-deposited film through changes in the laser flow, background pressure, target-substrate distance and species energy. In vacuum and helium atmosphere at different pressures, Saidani *et al.* prepared different materials using PLD (26). The surface of the rhodium film under vacuum was dense and smooth, while the surface of rhodium film prepared under helium atmosphere had porous nanostructure as a result of agglomerated phase particles.

2.3 Electrodeposition

Electrodeposition is a versatile technique by which a thin metallic layer can be obtained on the surface of a metal substrate by simple electrolysis of an aqueous solution containing the desired metal ion or its complex (27–29). The former two processes require a vacuum condition and high-cost devices (14, 15). Electrodeposition could be an alternative to produce a pure film on the surface of a conductive material at low temperature in aqueous solutions (30–33).

Electrodeposition offers several important advantages compared to the above two processes (34–37): (i) a relatively low-cost process; (ii) fairly simple and available equipment; (iii) porous, geometrically complex, or non-line-of-sight surfaces can be coated; (iv) the relatively low deposition temperature allows the formation

of highly crystalline films, with possibly lower residual stresses; (v) the thickness, composition and microstructure of the film can be controlled precisely. In aqueous solutions, rhodium's most stable oxidation state is +3, which forms complex ions readily. Rhodium deposition is usually electroplated from sulfate (38–41), nitric acid (42), phosphate or sulfate-phosphate baths (43). Rhodium metal complex baths have been reported based on citric, tartaric, lactic and boric acids, alkaline phosphate and aminonitrates (44). In rhodium sulfate solutions the species present are mostly $\text{Rh}(\text{H}_2\text{O})_6^{3+}$ and sometimes species like $\text{Rh}(\text{SO}_4)_3^{3-}$ are also observed. Several examples across the literatures are summarised in **Table III**. The non-exhaustive survey proposed here highlights and discusses the variety of rhodium solvents used and reaction conditions reported.

Oliveira *et al.* studied rhodium film electrodeposited on a polycrystalline platinum electrode in HClO_4 solutions and determined the main characteristics related to oxide formation on rhodium. The results demonstrated that Rh_0 adatoms were stable on platinum in the potential range investigated at different saturation coverages (36). Kibler *et al.* investigated the electrochemical deposition of rhodium on gold (111) by cyclic voltammetry and found that small three-dimensional (3D) clusters were formed (43). Yamazaki *et al.* reported a process for preparing rhodium nitrate solution and showed that rhodium deposits increased with the increase of applied cathodic potential (46). Pletcher and Urbina investigated electrodeposition of rhodium films from chloride and sulfate solutions and showed that strong acid medium led to a decrease in current efficiency (31, 32). It was possible to achieve 100% current efficiency keeping pH value in the range of pH 2–4. Mech *et al.* studied the mechanism and kinetics of rhodium(III) complexes using electroreduction in chloride solutions at pH 3.0 (37). These studies show that a higher current density or a higher temperature result in a faster plating process. For electrodeposition, processing parameters such as substrate, pH, current density and deposition potential are important to influence electrodeposition of the film. The bath temperature is also important. A rise in bath temperature causes a decrease in cathode polarisation. Cathode efficiency could be improved with increasing electrolyte bath temperature. However, it is easy to form coarse crystals and pores due to fast crystal growth rate at high temperature. Current density is another important

Table III Comparisons of Rhodium Electrolyte Types, Deposition Parameters and Surface Properties (40)

Electrolyte types	Deposition parameters			Substrates	Film quality	References
	T, °C	j, A cm ⁻²	pH			
Sulfate	40	0.08	1.2	SS304	Uniform, bright	(28)
	50	0.004–0.02	–	Brass cylinders	2.5 µm thickness and small humps	(30)
	25	0.001	3.3	Cu	Uniform, bright, highly reflecting	(31, 32)
	40–55	0.005–0.015	0.1–2	Ag/Ni/Au	Ductile, adherent film	(37)
	30–70	0.005–0.025	0.1–0.6	Ti	High adhesion and brightness	(34)
Chloride	20–40	0.0001–0.002	3.3	Cu	Uniform, bright	(31)
	25	0.0005	2.4–4	Carbon/Cu	Overlapping hemispheres	(32)
	22	0.5	–	Pt	A stable layer	(36)
	25	0.04	3	Au	No more information	(37)
	22			Ti	Good stability for OER	(38)
Phosphate	45–50	0.05	–	Ni	Thick film with cracks	(33)
	40	6	–	Metals	Bright white films	(44)
Phosphate-sulfate	50	0.013–0.02	–	Brass cylinders	2.5 µm thickness and rough surface	(30)
	40–50	0.02–0.1	–	Ni	Bright without cracks	(45)
	20–60	0.0064–0.1274	–	Cu-Zn	Uniform and good adhesion	(43)
Nitrate	25–50	0.03–0.5	–	Carbon fibre	Poorly reproducible, 30% deposition degree	(42)

variable which affects grain growth and amount of nucleation. Baraka *et al.* studied rhodium film electrodeposited on titanium substrates from a sulfate bath (34). Rhodium deposits formed on the substrates with high adhesion, brightness and current efficiency of 92.05% at optimal deposition conditions of pH 0.1, current density 25 mA cm⁻² and temperature 30°C. Sadeghi *et al.* concluded that the quality of rhodium deposits from a sulfate bath were comparable with those obtained from commercially available baths. The optimal deposition conditions for electrodeposition were pH 2.0 and current density 8.5 mA cm⁻² (47).

The electrochemical reaction is heterogeneous and includes both material transfer and electrochemical reaction, thus it is important to investigate the reaction mechanism to ensure optimal process conditions. **Figure 6** shows SEM images of cross-section and line energy dispersive spectrometry (EDS) patterns of film deposited at current density 0.1274 A cm⁻², bath temperatures 20°C and 50°C. The bonding between the film and substrate was good. The thickness of the film is about 1.6 µm and the structure is homogeneous, with a tight bond and no evidence of delamination. Copper and zinc decrease rapidly at the interface and the

film only consists of rhodium (40). Temperature plays an important role in deposition rate and film thickness. The crystallinity of the film changed a little with increase in bath temperature. The optimal electrodeposition conditions were pH 2.0, current density 8.5 mA cm⁻² and bath temperature 50°C.

With the development of science and technology, the demand for rhodium will also increase. Rhodium plating is clean, bright and white according to the characteristics of the plating layer and is very promising for both decorative and industrial applications.

2.4 Other Wet Chemical Synthesis

Wet chemical methods can control the size and shape of various NMNPs by controlling the reaction kinetics and thermodynamics. In recent years, wet chemical methods to modulate crystal growth kinetics include modified polyol methods, seed growth methods and organometallic methods in addition to electrochemical deposition.

The synthesis of NMNPs using a polyol process is a solution-based method to prepare colloidal NMNPs for catalytic applications. To produce

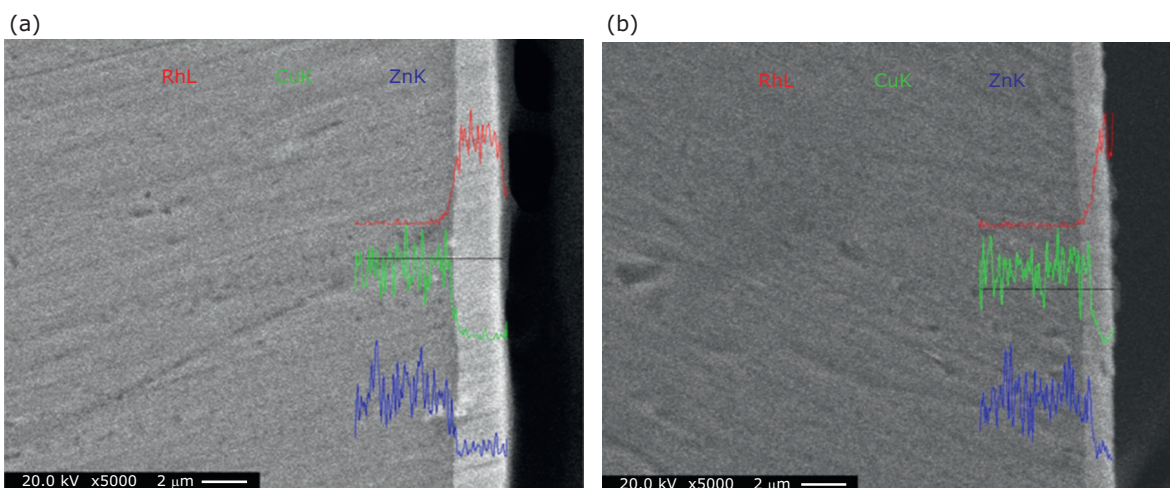


Fig. 6. Cross-sectional SEM images and line EDS patterns of rhodium film deposited at $j = 0.127 \text{ A cm}^{-2}$: (a) $T = 20^\circ\text{C}$; (b) $T = 50^\circ\text{C}$ (40). Reproduced with permission from SNCSC

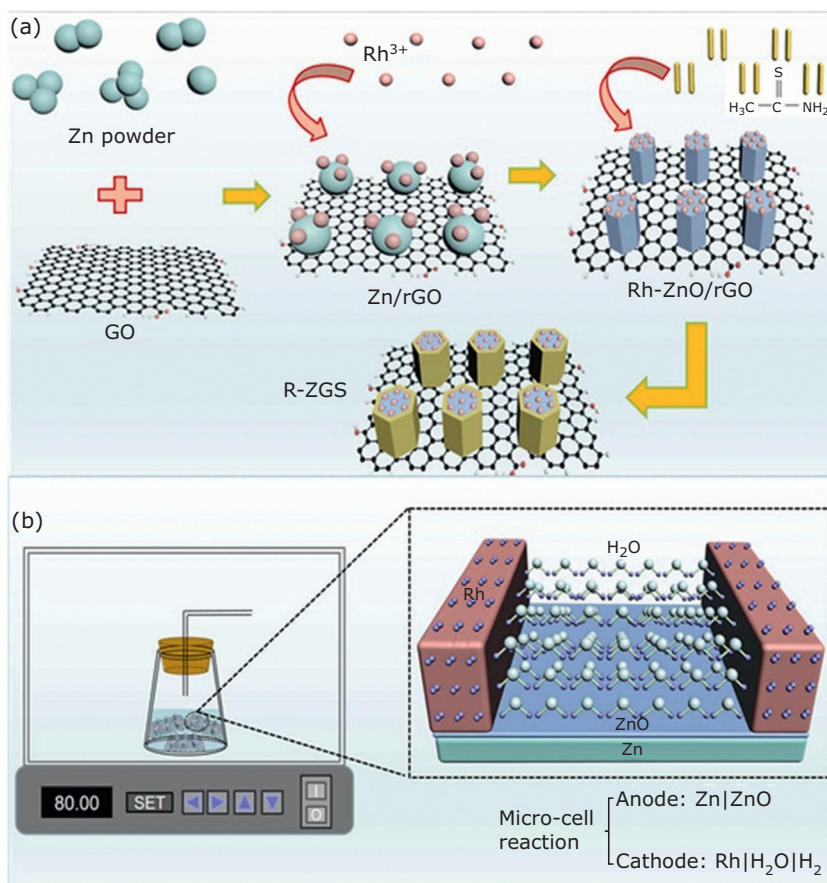


Fig. 7. (a) Synthetic strategy of the R-ZGS heterostructure; (b) diagram of rhodium-induced micro-cell growth. Reprinted from (50) with permission from Elsevier

metal colloids, organometallic compounds or salt precursors are usually heated in the presence of a stabiliser in a high boiling point polyol as solvent and reducing agent. Toshima and co-workers first reported their observations on the colloidal dispersion of rhodium NPs in the late

1970s (48). Rhodium NPs with a diameter of 40 Å were prepared by refluxing a mixture of polyvinyl alcohol and RhCl_3 in methanol-water. Bundli *et al.* synthesised platinum-rhodium NPs by polyol synthesis under inert conditions (argon, AGA) (49). Platinum(II)-acetylacetonate and

rhodium(III)-acetylacetonate were dissolved at room temperature in 1,4-butanediol and kept in four necked flasks under vigorous stirring, followed by addition of polyvinylpyrrolidone (PVP, $M_w = 10,000$) in a metal/PVP (monomer) molar ratio of 0.01:1. Bimetallic platinum-rhodium nanoparticles with controlled composition were obtained.

The seed growth method is a promising two-step process that separates thermally disfavoured nucleation processes from subsequent spontaneous growth steps by adding monomers to existing nanoparticles. Liang *et al.* fabricated Rh-ZnO/rGO/ZnS (abbreviated as R-ZGS) (rGO = reduced graphene oxide, GO = graphene oxide) heterostructure by rhodium-induced *in situ*

micro-cell growth and the kinetic ion-exchange process (50). The synthesis strategy is segmented into two parts: rhodium-induced micro-cell reaction and a dynamic ion-exchange process (**Figure 7(a)**). First, zinc powder can reduce GO to construct Zn/rGO. Rh^{3+} ion is reduced to rhodium through the substitution reaction and then locates on the surface of the zinc powder. As shown in **Figure 7(b)**, a micro-cell with $Rh=H_2O=H_2$ as the cathode and Zn/ZnO as the anode is formed in the system, where the rGO substrate facilitates smooth carrier transfer. With continuous progress of the reaction, zinc powder is continuously converted into ZnO and H_2 bubbles are continuously generated until the zinc powder is completely converted into ZnO. Thioacetamide was

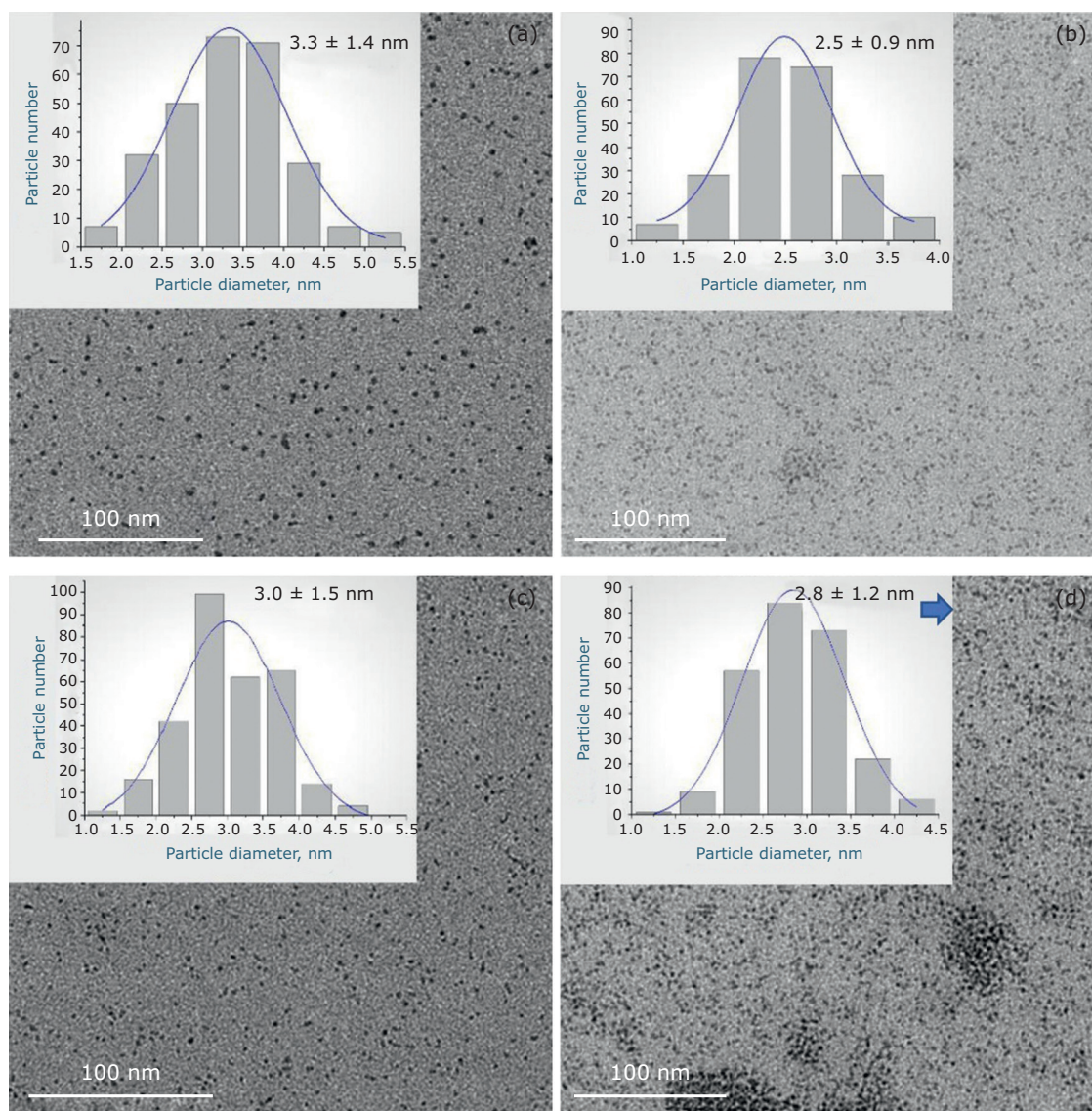


Fig. 8. TEM images of: (a) Pd-PVP; (b) Pd₂Rh₈-PVP; (c) Pd₅Rh₅-PVP; (d) Pd₈Rh₂-PVP nanoparticles with corresponding size histograms. Reprinted from (52) with permission from Elsevier

selected as the sulfur source to form the R-ZGS heterostructure. Finally, the interface-optimised R-ZGS was successfully fabricated for efficient water splitting driven by solar energy.

Organometallic derivatives, for example Rh(acac)₃, are widely used as precursors for the synthesis of monodispersed rhodium NPs (51). Zacahua-Tlacuatl *et al.* synthesised hemispherical PdRh NPs below 5 nm using organometallic precursors as raw materials and PVP as stabiliser (52). Well-dispersed nanostructures with hemispherical shape can be observed on TEM images (**Figure 8**), indicating that the PVP polymer matrix acts as an effective stabiliser and prevents the agglomeration of NPs. Having well-dispersed and small NPs is a promising feature for catalysis due to the large number of potential active catalytic sites.

Part II of this review will cover applications in industries such as optical mirrors, electrical applications, sensors and anticancer drugs (53).

References

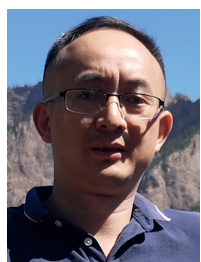
1. S. Mourdikoudis, R. M. Pallares, N. T. K. Thanh, *Nanoscale*, 2018, **10**, (27), 12871
2. P. Losch, W. Huang, E. D. Goodman, C. J. Wrasman, A. Holm, A. R. Riscoe, J. A. Schwalbe, M. Cargnello, *Nano Today*, 2019, **24**, 15
3. J. Quinson, *Adv. Colloid Interface Sci.*, 2022, **303**, 102643
4. J. Krajczewski, R. Ambroziak, A. Kudelski, *RSC Adv.*, 2022, **12**, (4), 2123
5. L. Xu, D. Liu, D. Chen, H. Liu, J. Yang, *Heliyon*, 2019, **5**, (1), e01165
6. S. Xie, S.-I. Choi, X. Xia, Y. Xia, *Curr. Opin. Chem. Eng.*, 2013, **2**, (2), 142
7. W. Zang, G. Li, L. Wang, X. Zhang, *Catal. Sci. Technol.*, 2015, **5**, (5), 2532
8. L. Marot, G. Covarel, M.-H. Tuilier, R. Steiner, P. Oelhafen, *Thin Solid Films*, 2008, **516**, (21), 7604
9. S. Rai, U. Shaislamov, J. K. Yang, S. Saud, W. A. Muhammed, H. J. Lee, *J. Korean Phys. Soc.*, 2019, **75**, (8), 644
10. G. Taylor, R. Paladines, A. Marti, D. Jacobs, S. Tint, A. Fones, H. Hamilton, L. Yu, S. Amini, J. Hettinger, *Electrochim. Acta*, 2021, **394**, 139118
11. L. Marot, G. De Temmerman, P. Oelhafen, G. Covarel, A. Litnovsky, *Rev. Sci. Instrum.*, 2007, **78**, (10), 103507
12. L. Marot, G. De Temmerman, V. Thommen, D. Mathys, P. Oelhafen, *Surf. Coatings Technol.*, 2008, **202**, (13), 2837
13. L. Marot, R. Steiner, M. Gantenbein, D. Mathys, E. Meyer, *J. Nucl. Mater.*, 2011, **415**, (1), S1203
14. A. Uccello, B. Eren, L. Marot, D. Dellasega, A. Maffini, R. Steiner, D. Mathys, E. Meyer, M. Passoni, *J. Nucl. Mater.*, 2014, **446**, (1–3), 106
15. A. T. T. Mostako, A. Khare, C. V. S. Rao, S. Vala, T. K. Basu, P. M. Raole, R. Makwana, *J. Nucl. Mater.*, 2014, **446**, (1–3), 63
16. A. De Bonis, A. Santagata, M. Sansone, J. V. Rau, T. Mori, R. Teghil, *Appl. Surf. Sci.*, 2013, **278**, 321
17. A. T. T. Mostako, A. Khare, C. V. S. Rao, S. Vala, R. J. Makwana, T. K. Basu, *Nucl. Instrum. Meth. Phys. Res. Sect. B: Beam Interact. Mater. Atoms*, 2015, **342**, 150
18. A. T. T. Mostako, A. Khare, C. V. S. Rao, P. M. Raole, S. Vala, S. Jakhar, T. K. Basu, M. Abhangi, R. J. Makwana, *J. Nucl. Mater.*, 2012, **423**, (1–3), 53
19. D. S. Negi, A. Roy, B. Loukya, K. Dileep, S. Shetty, N. Kumar, P. S. A. Kumar, R. Datta, *J. Cryst. Growth*, 2014, **394**, 112
20. A. Usman, M. S. Rafique, M. Khaleeq-ur-Rahman, K. Siraj, S. Anjum, H. Latif, T. M. Khan, M. Mehmood, *Mater. Chem. Phys.*, 2011, **126**, (3), 649
21. A. Uccello, A. Maffini, D. Dellasega, M. Passoni, *Fusion Eng. Des.*, 2013, **88**, (6–8), 1347
22. A. T. T. Mostako, C. V. S. Rao, A. Khare, *Rev. Sci. Instrum.*, 2011, **82**, (1), 013101
23. A. Uccello, D. Dellasega, S. Perissinotto, N. Lecis, M. Passoni, *J. Nucl. Mater.*, 2013, **432**, (1–3), 261
24. M. Passoni, D. Dellasega, G. Grosso, C. Conti, M. C. Ubaldi, C. E. Bottani, *J. Nucl. Mater.*, 2010, **404**, (1), 1
25. P. Mertens, R. Boman, S. Dickheuer, Y. Krasikov, A. Krimmer, D. Leichtle, K. Liegeois, C. Linsmeier, A. Litnovsky, O. Marchuk, M. Rasinski, M. De Bock, *Fusion Eng. Des.*, 2019, **146**, (B), 2514
26. F. Saidani, D. Rochefort, M. Mohamedi, *Electrocatalysis*, 2011, **2**, (2), 114
27. R. Li, Y. Li, P. Yang, D. Wang, H. Xu, B. Wang, F. Meng, J. Zhang, M. An, *J. Energy Chem.*, 2021, **57**, 547
28. B. K. Devendra, B. M. Praveen, V. S. Tripathi, G. Nagaraju, D. H. Nagaraju, K. O. Nayana, *Inorg. Chem. Commun.*, 2021, **134**, 109065
29. B. K. Devendra, B. M. Praveen, V. S. Tripathi, D. H. Nagaraju, M. Padaki, H. P. Nagaswarupa, R. H. Krishna, *Appl. Surf. Sci. Adv.*, 2022, **12**, 100320
30. H. C. Angus, *Trans. IMF*, 1965, **43**, (1), 135
31. D. Pletcher, R. I. Urbina, *J. Electroanal. Chem.*, 1997, **421**, (1–2), 137
32. D. Pletcher, R. I. Urbina, *J. Electroanal. Chem.*, 1997, **421**, (1–2), 145

33. F. H. Reid, *Trans. IMF*, 1955, **33**, (1), 105
34. A. M. Baraka, H. A. Hamed, H. H. Shaarawy, *Anti-Corros. Meth. Mater.*, 2002, **49**, (4), 277
35. J. Janata, *Angew. Chem.*, 2011, **123**, (41), 9710
36. R. T. S. Oliveira, M. C. Santos, L. O. S. Bulhões, E. C. Pereira, *J. Electroanal. Chem.*, 2004, **569**, (2), 233
37. K. Mech, P. Żabiński, R. Kowalik, M. Wojnicki, *Surf. Coat. Technol.*, 2014, **258**, 72
38. R. Rudolf, B. Budić, D. Stamenković, M. Čolić, A. Ivanič, B. Kosec, *Metalurgija*, 2013, **52**, (3), 337
39. V. K. Varentsov, V. I. Varentsova, *Russ. J. Electrochem.*, 2003, **39**, (6), 703
40. W. Wu, J. Liu, Y. Zhang, X. Wang, Y. Zhang, *J. Appl. Electrochem.*, 2019, **49**, (10), 1043
41. B. K. Devendra, B. M. Praveen, V. S. Tripathi, H. P. P. Kumar, K. R. Chethana, *J. Indian Chem. Soc.*, 2022, **99**, (6), 100466
42. A. Tabet-Aoul, M. Mohamedi, *Thin Solid Films*, 2013, **534**, 270
43. L. A. Kibler, M. Kleinert, D. M. Kolb, *J. Electroanal. Chem.*, 1999, **467**, (1-2), 249
44. H. Panda, "Handbook on Electroplating with Manufacture of Electrochemicals", Asia Pacific Business Press Inc, Delhi, India, 2017
45. A. M. Weisberg, *Metal Finish.*, 1999, **97**, (1), 297
46. H. Yamazaki, Tanaka Kikinzoku Kogyo KK, Japan, 'Process for Preparing Rhodium Nitrate Solution', *US Patent*, 4,844,879; 1989
47. M. Sadeghi, P. Van den Winkel, H. Afarideh, M. Haji-Saeid, *J. Radioanal. Nucl. Chem.*, 2005, **262**, (3), 665
48. H. Hirai, Y. Nakao, N. Toshima, *J. Macromol. Sci. Part A Chem.*, 1978, **12**, (8), 1117
49. S. Bundli, P. Dhak, M. Jensen, A. E. Gunnæs, P. D. Nguyen, H. Fjellvåg, A. O. Sjøstad, *J. Alloys Compd.*, 2019, **779**, 879
50. S. Liang, J. Wang, Q. Lin, R. Zhang, X. Wang, *J. Alloys Compd.*, 2022, **904**, 164021
51. Q. Shuai, L. Yang, X. Guo, O. Baslé, C.-J. Li, *J. Am. Chem. Soc.*, 2010, **132**, (35), 12212
52. G. Zacahua-Tlacuati, E. Ramírez-Meneses, A. Manzo-Robledo, A. M. Torres-Huerta, I. Betancourt, K. Philippot, M. Ibrahim, M. A. Domínguez-Crespo, *Int. J. Hydrogen Energy*, 2023, **48**, (23), 8450
53. Y. Zhou, W. Wu, Q. Wang, L. Wang, *Johnson Matthey Technol. Rev.*, 2024, **68**, (1), 102

The Authors



Yicheng Zhou is a Master's research scholar under the guidance of Wangping Wu in the School of Mechanical Engineering and Rail Transit, Changzhou University, China. He received his BA from Suzhou University of Science and Technology, China, in 2020. His current research focuses on catalysis, energy, electrochemistry and corrosion. He has experience and knowledge in the preparation of thin films and nanoparticles by electrodeposition. He had the National scholarship for Postgraduates in 2023 and has published seven papers in peer-reviewed international journals and one patent.



Wangping Wu received his PhD in Materials Processing Engineering from Nanjing University of Aeronautics and Astronautics, China, in 2013. He joined the Tel Aviv University, Israel, as a Postdoctoral Fellow from October 2013, and joined the Hochschule Mittweida University of Applied Sciences, Germany, and Technische Universität Chemnitz, Germany, from September 2019 as a visiting scholar by the support of China Scholarship Council (CSC). He then joined the Engle Machinery Co, Ltd from January 2023 as a senior engineer. He currently works as an Associate Professor at the School of Mechanical Engineering and Rail Transit, Changzhou University, China. His research focuses on the synthesis, characterisation and performance of films and coatings of the noble metals and their alloys, nanopowders dispersed in polymer and electrochemical additive manufacturing. He has published over 100 papers in peer-reviewed international journals, over 10 invent patents and two books.



Qinqin Wang received her PhD in Materials Science and Engineering from Changzhou University, China, in 2022. She engaged in the photovoltaic industry for more than ten years and worked in LONGi Solar Technology Co, Ltd as a senior chief engineer. She currently works as a lecturer at the Institute of Technology for Carbon Neutralition, School of Mechanical Engineering, Yangzhou University, China. Her research focuses on the industrial application of high-efficiency crystalline silicon solar cell, structural design of tandem cell, optical and electrical matching and other issues. She has published over 20 papers in peer-reviewed international journals and over 10 invent patents.



Liangbing Wang is a Master's research scholar who graduated from the School of Materials Science and Technology, Nanjing University of Aeronautics and Astronautics. He is currently the executive deputy general manager of AVIC Surface Treatment Technology (Tianjin) Co, Ltd. He has been engaged in material heat treatment and surface treatment. He carries out basic research into type selection, heat treatment process, corrosion and protection of metal materials, process management, forward process design and process verification. He has published over 10 papers in peer-reviewed international journals and eight patents.